Original

Li, Y.; Lu, X.; Serdechnova, M.; Blawert, C.; Zheludkevich, M.L.; Qian, K.; Zhang, T.; Wang, F.:

Incorporation of LDH nanocontainers into plasma electrolytic oxidation coatings on Mg alloy.

In: Journal of Magnesium and Alloys. (2021)

First published online by Elsevier: 04.09.2021

https://dx.doi.org/10.1016/j.jma.2021.07.015

Available online at www.sciencedirect.com
ScienceDirect
Journal of Magnesium and Alloys xxx (xxxx) xxx
www.elsevier.com/locate/jma

Full Length Article

Incorporation of LDH nanocontainers into plasma electrolytic oxidation coatings on Mg alloy

Yan Li[a], Xiaopeng Lu[a,*], Maria Serdechnova[b], Carsten Blawert[b], Mikhail L. Zheludkevich[b,c], Kun Qian[d], Tao Zhang[a], Fuhui Wang[a]

[a] *Shenyang National Laboratory for Materials Science, Northeastern University, 3-11 Wenhua Road, Shenyang 110819, China*
[b] *Institute of Surface Science, Helmholtz-Zentrum Hereon, Geesthacht 21502, Germany*
[c] *Institute of Materials Research, Faculty of Engineering, University of Kiel, Kaiserstraβe 2, Kiel 24143, Germany*
[d] *School of Materials Science and Engineering, Southeastern University, Nanjing 211189, China*

Received 25 February 2021; received in revised form 15 June 2021; accepted 16 July 2021
Available online xxx

Abstract

In-situ incorporation of layered double hydroxides (LDH) nanocontainers into plasma electrolytic oxidation (PEO) coatings on AZ91 Mg alloy has been achieved in the present study. Fumarate was selected as Mg corrosion inhibitor for exchange and intercalation into the nanocontainers, which were subsequently incorporated into the coating. It was found that the thickness and compactness of the coatings were increased in the presence of LDH nanocontainers. The corrosion protection performance of the blank PEO, LDH containing PEO and inhibitor loaded coatings was evaluated by means of polarization test and electrochemical impedance spectroscopy (EIS). The degradation process and corrosion resistance of PEO coating were found to be greatly affected by the loaded inhibitor and nanocontainers by means of ion-exchange when corrosion occurs, leading to enhanced and stable corrosion resistance of the substrate.

Keywords: Magnesium; Layered double hydroxides; Inhibitor; Plasma electrolytic oxidation; Nanocontainer.

1. Introduction

Magnesium (Mg) and its alloys are considered as promising metallic materials for aeronautic, automotive and biomedical applications due to their excellent strength-to-weight ratio and biocompatibility [1–5]. Nevertheless, poor corrosion resistance is an important obstacle which limits their utilization [6–10]. Surface treatment processes (chemical conversion coating, [11] electrochemical plating, [12] organic coating [13] and plasma electrolytic oxidation (PEO) [14,15] have been developed and optimized to improve the corrosion performance of Mg alloys. Among these techniques, PEO is an advanced anodizing process to form ceramic-like oxide coatings on the surface of light metals (Mg, Al and Ti) and confer enhanced corrosion and wear resistance [16–20]. Nevertheless, the coatings normally have high porosity owing to discharges and gas evolution accompanied with coating growth, which can deteriorate the corrosion property [21,22]. Plenty of studies have been carried out to increase the compactness and range of coating composition to improve the barrier property of the layer [23–25].

Corrosion inhibitors can be added into the open pores of PEO coatings by post-treatment processes to achieve long-term corrosion protection for Mg alloys [26–32] 3-methysalicylate [33] and 1, 2, 4-triazole [34] were impregnated into the porous layer and subsequently sealed by an epoxy layer through dip-coating process. It was found that the hybrid coating can significantly enhance the corrosion performance of Mg surface. However, the coating preparation process is complex and might lead to a nonuniform composite layer and decrease the adhesion of the coating with the sub-

* Corresponding author.
E-mail address: luxiaopeng@mail.neu.edu.cn (X. Lu).

https://doi.org/10.1016/j.jma.2021.07.015

Please cite this article as: Y. Li, X. Lu, M. Serdechnova et al., Incorporation of LDH nanocontainers into plasma electrolytic oxidation coatings on Mg alloy, Journal of Magnesium and Alloys, https://doi.org/10.1016/j.jma.2021.07.015

strate. Therefore, *in-situ* incorporation of nanocontainers can be considered as a strategy to add Mg inhibitors into PEO coatings to provide active corrosion protection. Sun et al.[35] loaded benzotriazole (BTA) to halloysite nanotubes (HNT) and afterwards incorporated the containers into PEO coated AM50 Mg alloy and found that the corrosion resistance of the coating was greatly enhanced after loading BTA into the layer.

In recent years, layered double hydroxide (LDH) have attracted attention as effective nanocontainers for corrosion inhibitors [36–39]. LDH belongs to hydrotalcite-group of compounds, which are typically composed of mixed metal M^{II}-M^{III} hydroxide layers [40–42]. Corrosion inhibitors can be exchanged and intercalated into the LDH galleries as charge compensating anions and are subsequently released when corrosion occurs. Some studies have been focused on formation of composite PEO-LDH coating system by means of post-treatment process to enhance the corrosion resistance of Mg and Al substrates. Serdechnova and Mohedano produced LDH layer on top of PEO coating on Al alloy and subsequently loaded vanadate ions as corrosion inhibitor. [43,44]. It was found that the composite layer with exchanged corrosion inhibitor greatly enhanced the corrosion resistance of the coating. Wu et al.[45] developed MgAl LDH layer on anodized coating on AZ31 Mg alloy. It was found that the sources of Mg^{2+} and Al^{3+} cations were originated from dissolution of the Mg substrate and degradation of the anodic films. The same group tried to intercalate phytic acid (PA) into the coating via ion-exchange reaction and proposed that the inhibitor modified LDH/PEO composite coating showed enhanced corrosion resistance and self-healing ability [46]. Petrova et al. [47,48] found that it was possible to grow LDH at ambient pressure on PEO treated Mg alloy in the presence of chelating agents, which can avoid using hydrothermal autoclave conditions.

Nevertheless, *in-situ* incorporation of inhibitor containing LDH nanocontainers into PEO coating appears to be simpler and more efficient compared to the reported two-step preparation process. Fumaric acid was found to show high corrosion inhibition efficiency on Mg alloy, which was proposed due to chemisorption at the $MgO/Mg(OH)_2$ surface by carboxylate bond formation [49,50]. Therefore, LDH was used as nanocontainer in the present work to load fumaric acid as Mg inhibitor, which was subsequently incorporated into PEO coating during coating formation process. Parental LDH-nitrate particles were also added into PEO electrolyte to study the influence of inhibitors on the corrosion performance of the coatings.

2. Material and methods

2.1. Material and PEO treatment

Die-cast AZ91 Mg alloy was used as the substrate to produce PEO coatings. The chemical composition of the alloy is listed in Table 1. Specimens with dimension of $15 \times 15 \times 6$ mm^3 were ground and ultrasonically cleaned with distilled water prior to PEO processing. Zn-Al LDH ($Zn_2Al(NO_3)(OH)_6 \cdot 2H_2O$, water based slurry, 400–800 nm, Smallmatek, Portugal) nanocontainers were used to load Mg corrosion inhibitor [51]. 5 g/L fumaric acid ($C_4H_4O_4$, Sinopharm Chemical Reagent Co., Ltd) was neutralized by NaOH to form sodium fumarate, which was then mixed with 10 g/L LDH for exchange of inhibitor under a magnetic stirrer with a speed of 500 rpm/min at room temperature for 5 h. Afterwards, the inhibitor containing LDH nanocontainer was added to a slightly alkaline PEO electrolyte, which was composed of 10–20 ml/L phosphoric acid and 100–180 ml/L ammonia. PEO treatment was carried out in a constant current density mode (2 A/dm^2) to 400 V with a pulsed power supply. The respective samples are named as PEO, PEO-LDH (with addition of parental LDH) and PEO-LDH-FA (fumarate containing LDH).

Table 1
Chemical composition of AZ91 Mg alloy.

Element	Al	Zn	Mn	Fe	Si	Ni	Mg
Content (wt.%)	9.23	0.735	0.21	0.0014	0.03	0.0018	balance

2.2. Characterization of LDH nanocontainer and PEO coatings

The microstructure and morphology of the coatings were analyzed by scanning electron microscope (SEM, JSM-7001F, JEOL, Japan). Surface topography and roughness (R_a) of coatings were investigated by laser confocal microscopy (FV1200, Olympus Corporation, Japan). Electron probe microanalysis (EPMA1720, Shimadzu, Japan) was used to investigate the elemental composition of the coatings. The composition of LDH nanocontainer was analyzed using Bruker D8 Advance diffractometer, while phase composition of the PEO coatings was examined using SmartLab X-ray diffractometer (Rigaku, Japan). In both cases Ni-filtered Cu Kα radiation in a 2-theta range between 5 and 70° was used. The selected measurement steps were defined as 0.02° per step with exposure time of 1 s per step. The inhibitor in the samples was characterized by reference via total reflection Fourier transform infrared spectroscopy (Nicolet 6700, Thermofisher, USA).

2.3. Electrochemical corrosion measurements

The corrosion properties of the coatings were evaluated via performing electrochemical corrosion tests in 0.5 wt% NaCl solution using potentiostat (P4000, Ametek, USA). The measurements were performed in a conventional three-electrode cell system including a saturated calomel as the reference electrode, a platinum electrode as the counter electrode and the coatings as the working electrode. Electrochemical impedance spectroscopy (EIS) was measured with 20 mV (peak-to-peak) sinusoidal perturbation in the frequency range from 100 kHz to 0.01 Hz. The blank coating was measured for 5 days due to rapid degradation of the layer, while the LDH containing coatings were tested for 10 days for EIS

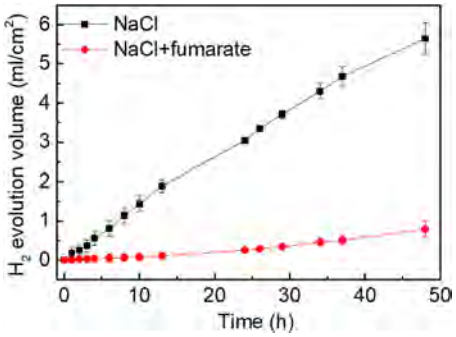

Fig. 1. H_2 evolution test of AZ91 Mg alloy immersed in 3.5 wt.% NaCl with and without addition of 0.05 mol/L fumarate.

measurement. Potentiodynamic polarization was performed from the open circuit potential (OCP) after stabilizing for 20 min to the cathodic and anodic direction with a scan rate of 0.333 mV/s.

3. Results and discussion

3.1. HE measurement

The hydrogen evolution test of Mg alloy in NaCl solution with and without addition of fumarate is displayed in Fig. 1. It can be seen that the corrosion rate of Mg was significantly reduced in the presence of corrosion inhibitor. The inhibition efficiency (η) of the inhibitor was calculated using Eq. (1). V_{HE} and V'_{HE} are the respective volume of the evolved H_2 after immersion in blank NaCl and inhibitor containing NaCl solution.

$$\eta = \frac{V_{HE} - V'_{HE}}{V_{HE}} \times 100\% \quad (1)$$

The inhibition efficiency of fumarate reaches 90%. The inhibition effect of the inhibitor is also demonstrated by the surface morphology of the corroded samples (Fig. 2). Corrosion products are accumulated on the surface of the alloy and deep localized corrosion attack occur in the blank NaCl solution (Fig. 2a and c), while the corrosion layer appears to be dense and protective on the sample in the presence of inhibitor (Fig. 2b and d).

3.2. XRD of LDH nanocontainer before and after exchange with inhibitor

The XRD patterns of the parental Zn-Al LDH and after the intercalation of fumarate as corrosion inhibitor are illustrated in Fig. 3. The well-defined peaks at 9.93° and 19.92° correspond to the characteristic (003) and (006) reflections of parental LDH [44,52]. After the performed exchange reaction, these characteristic peaks are shifted to 10.35° and 20.93°, respectively, confirming the successful intercalation of fumarate anions into the LDH intergalleries. Important to highlight, that host LDH layers stay intact after the exchange process: the respective reflections (110) and (113) are clearly detectable at the same positions (see the inset in Fig. 3). Thus, it can

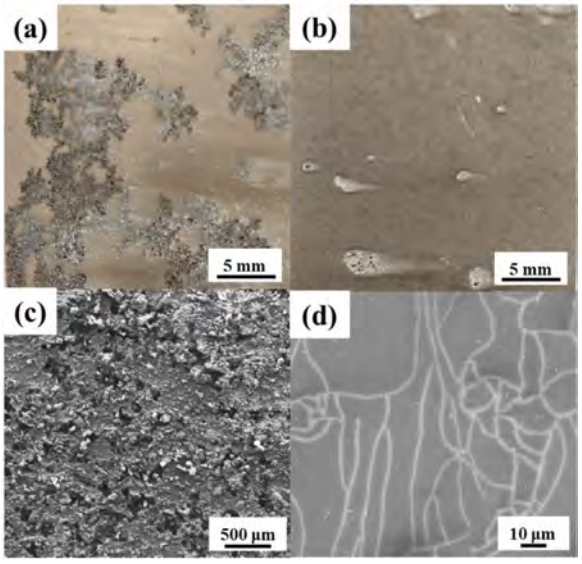

Fig. 2. Macroscopic and microscopic morphology of the samples immersed in blank NaCl solution (a and c) and fumarate containing NaCl solution (b and d) after corrosion test for 48 h.

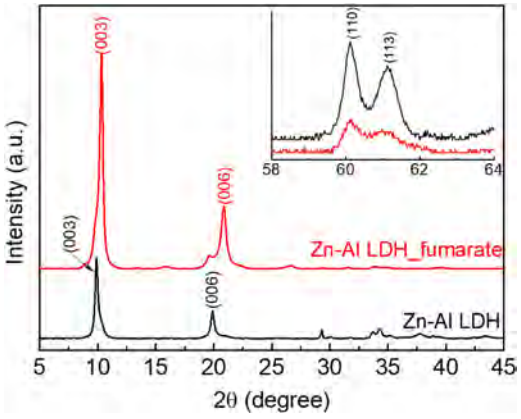

Fig. 3. XRD patterns of the parent Zn-Al LDH before and after anion exchange with fumarate.

be concluded that the corrosion inhibitor (fumarate) has been intercalated into the parental Zn-Al LDH nanocontainers.

3.3. Voltage-time response during coating formation process

Fig. 4 shows the evolution of the voltage as a function of treatment time during coating formation process. It seems that the initial stage of the coating growth is not affected by the presence of LDH nanocontainers in the electrolyte, while the voltage increases faster at the later stage, indicating that the barrier property of the coating is enhanced after incorporation of LDH. There is no remarkable difference between the treatments in electrolyte with LDH and inhibitor loaded LDH, which might be an indication that the fumarate is not leaching to the treatment electrolyte.

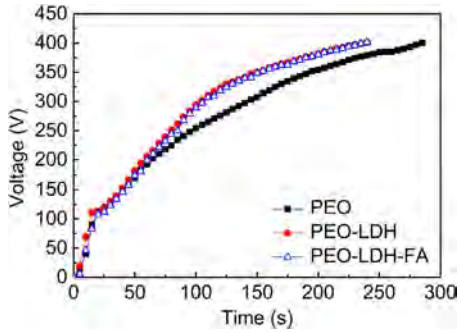

Fig. 4. Voltage vs. time plot during PEO processing in electrolytes with and without addition of LDH nanocontainer.

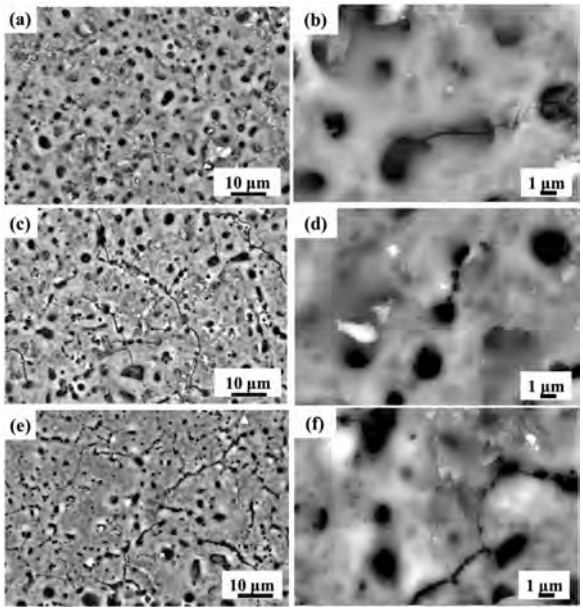

Fig. 5. Surface morphology of the PEO coatings (a) PEO (b) PEO-LDH and (c) PEO-LDH-FA.

Table 2
Surface compositions (at.%) of the coatings determined by EDS analysis.

Element	O	Mg	Al	P	Zn
PEO	57.72	23.36	1.27	17.59	0.06
PEO-LDH	60.16	19.49	2.68	15.25	2.42
PEO-LDH-FA	60.81	20.82	2.36	14.34	1.67

3.4. Microstructure and composition of the PEO coatings

The surface morphology and elemental composition of the coatings are shown in Figs. 5 and 6. It can be seen that the number of pores in the coating is slightly reduced after addition of LDH nanocontainers. The cracks appearing on the surface are more pronounced and the size of the micropores is constant or slightly decreased. As expected, the coatings consist of Mg, P, O and Al, which are the main elements of the electrolyte and substrate. Zn is only detected on the surface of coatings with addition of LDH nanocontainer, suggesting that the Zn-Al LDH particles have been incorporated into the layer. This can be further confirmed by Table 2. The

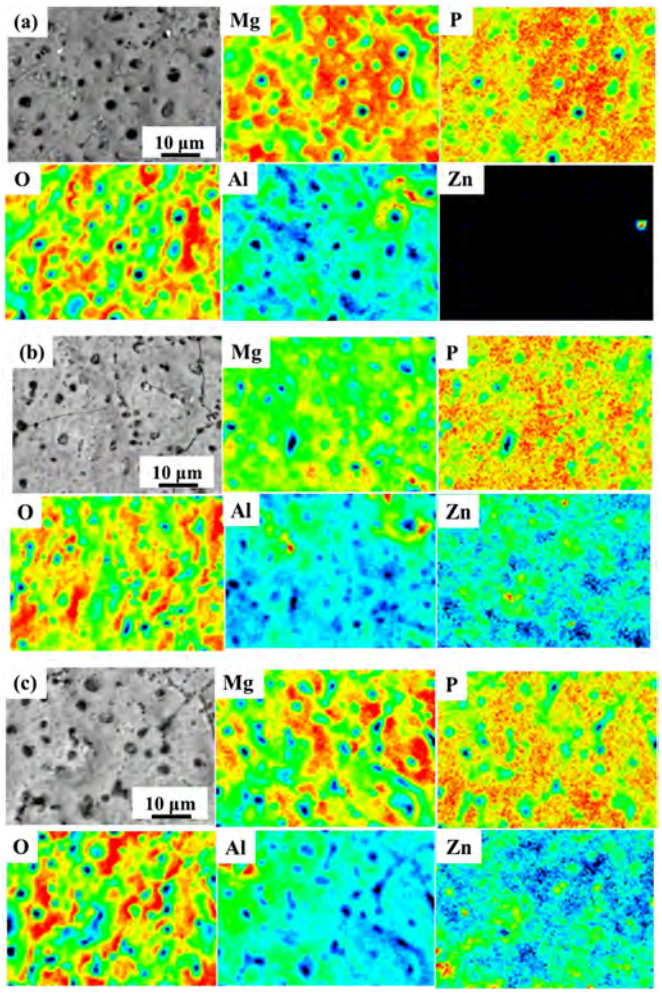

Fig. 6. Main elemental distribution (Mg, P, O, Al and Zn) on the coating surface (a) PEO, (b) PEO-LDH and (c) PEO-LDH-FA.

surface topography of the coatings is presented in Fig. 7. It is obvious that the surface roughness is changed after addition of LDH nanocontainers. The coating becomes smoother and the roughness (R_a) is decreased from approximately 2 to 1–1.2 μm. It can be inferred that the nanocontainers influence the coating formation process and have been incorporated into the layer.

The cross section and elemental distribution of the PEO coatings are shown in Fig. 8. Particularly, the addition of LDH and inhibitor have slightly increased the coating thickness from 20.5 ± 2 μm to 22.5 ± 1 μm and 21.5 ± 1 μm, respectively. Mg, P, Al and Zn elements were detected as the main elements in all coatings. Similar as for the surface, Zn is detected and distributed throughout the whole layer after incorporation of LDH nanocontainers. All the elements are uniformly distributed in the coating.

3.5. Phase composition of the PEO coatings

The phase composition of the coatings is shown in Fig. 9. It can be observable that the coatings are composed of MgO, $Mg_3(PO_4)_2$ and amorphous phase. The XRD patterns

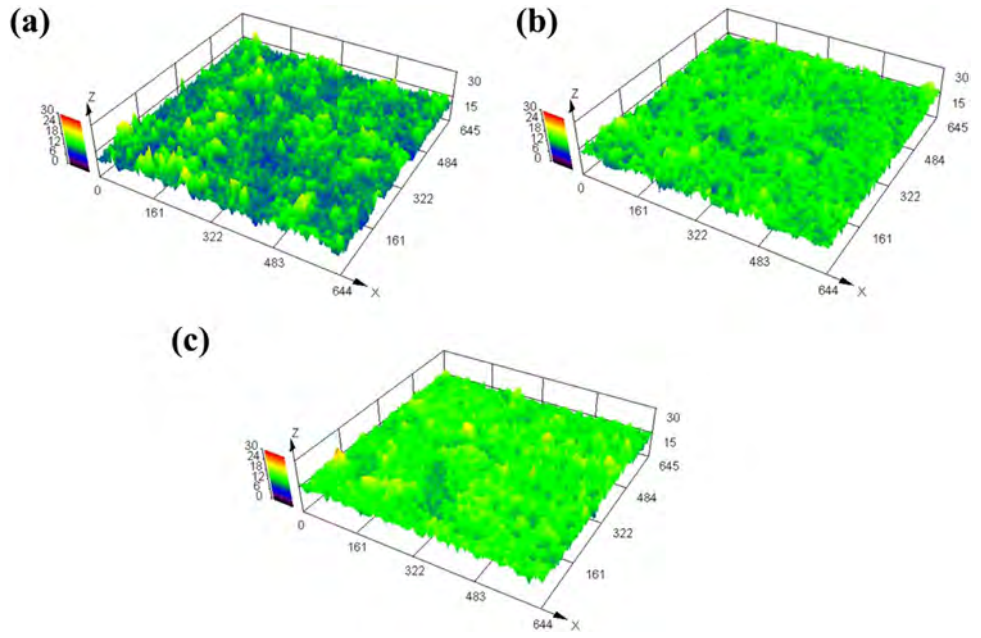

Fig. 7. 3D surface topography of the PEO coatings (a) PEO (b) PEO-LDH (c) PEO-LDH-FA.

Table 3
Fitted results of the impedance spectrum of the coatings.

Samples	Time (h)	CPE_c (μS $cm^{-2}s^n$)	n_1	R_c (Ω cm^2)	CPE_{dl} (μS $cm^{-2}s^n$)	n_2	R_{ct} (Ω cm^2)
PEO	24	8.31	0.91	2.56E4	290.8	0.56	2.31E4
	48	9.60	0.91	2.48E4	311.3	0.54	1.32E5
	72	4.49	0.95	272.2	4.07	0.93	1.68E4
	96	4.62	0.97	201.4	2.79	0.93	1.15E4
	120	1.06	0.93	66.34	7.01	0.93	1.04E4
PEO-LDH	24	5.96	0.86	6.78E4	358.7	0.82	1.09E4
	72	6.62	0.89	8.76E4	124.1	0.61	2.57E4
	144	7.24	0.90	8.29E4	124.8	0.63	2.75E4
	168	7.68	0.90	3.89E4	236.9	0.67	3.49E4
	240	8.11	0.90	6.28E4	276.6	0.78	2.71E4
PEO-LDH-FA	24	4.84	0.90	8.97E4	187.6	0.60	2.89E4
	72	6.22	0.91	6.28E4	199.5	0.63	1.59E4
	144	6.92	0.91	7.98E4	101.2	0.58	6.39E4
	168	7.52	0.91	4.88E4	190.8	0.65	3.47E4
	240	7.82	0.91	7.01E4	210.5	0.73	4.18E4

of LDH containing PEO coating exhibit identical peaks corresponding to (003) and (006) reflections of LDH in 9.56° and 21°. Moreover, the phase composition of the coating seems to be not affected after addition of corrosion inhibitors. The presence of LDH peaks indicate that the nanocontainers are inertly or only partly reactively incorporated into the coating.

ATR-FTIR was used to investigate the existence of inhibitors on the coating surface (Fig. 10). Carboxylate bond can be considered as sign for the corrosion inhibitor since fumarate is an olefin containing carboxylic acid salt. In the spectra of PEO-LDH-FA, the absorption peak at 1637.78 and 1383.43 cm^{-1} can be ascribed to asymmetric and symmetric carboxylate bonds in fumarate,[50] while the peaks at 3435.95 and 2919.65 cm^{-1} can be assigned to O–H, and C–H (stretch vibration) [53,54]. The peaks located at 567.62 cm^{-1} can be assigned to the stretching vibration of M-O (Al/Zn) in the LDH [55]. In contrast to the infrared spectrum of PEO-LDH coating, the signal of the carboxylate bonds in fumarate and PEO-LDH-FA are more pronounced, which suggests that the inhibitor was successfully incorporated into the layer.

3.6. Corrosion protection behavior of the PEO coatings

The polarization curves of the coatings measured in 0.5 wt% NaCl solution are presented in Fig. 11. The corrosion current density (i_{corr}) was calculated based on the polarization cathodic curve [56,57]. According to the polarization curves, the i_{corr} of PEO coating is reduced from 59.51 to 30.33 (PEO-LDH) and 14.81 $\mu A/cm^2$ (PEO-LDH-FA), indicating that the corrosion resistance of the layer is enhanced after addition of LDH nanocontainer. The corrosion potential of the coating becomes more noble (−1.51 V) after incorporation of corrosion inhibitor and nanocontainer. In addition, the anodic dissolution is significantly retarded according to the anodic

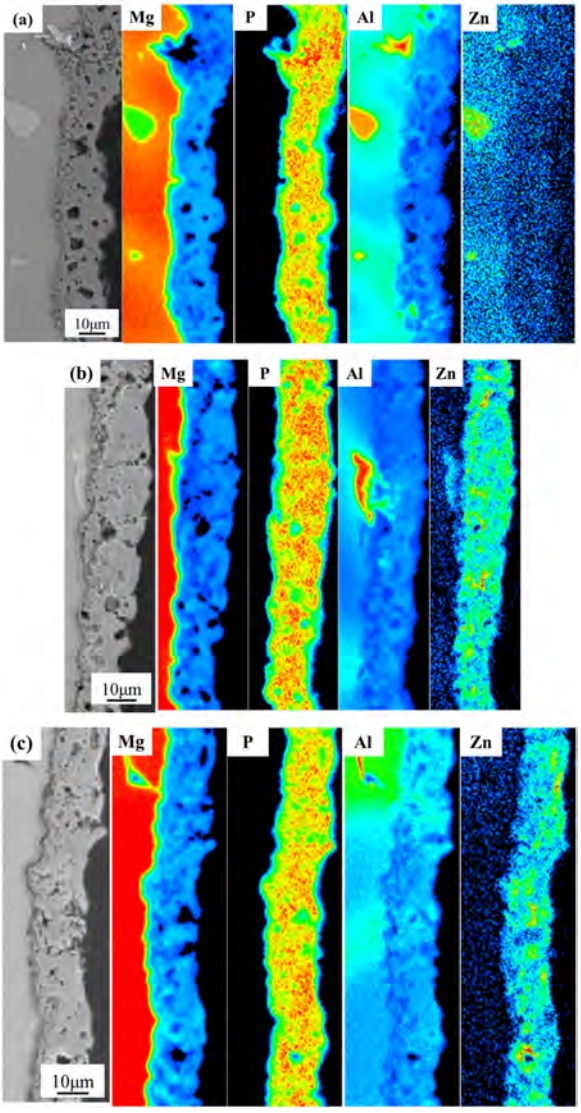

Fig. 8. Cross-sectional and main elemental distribution on the cross section of PEO coatings (a) PEO, (b) PEO-LDH and (c) PEO-LDH-FA.

polarization curve, which might be ascribed to the effect of inhibitors in the coating.

Long-term EIS test was performed to evaluate the degradation process of the PEO coatings (Fig. 12). The low frequency impedance of the blank PEO coating is found to be much lower in contrast with PEO-LDH and PEO-LDH-FA at the initial stage of corrosion test. It can be seen that the impedance of the blank coating degrades rapidly after immersion for 72 h (Fig. 12a) and therefore the coating was only tested for 5 days, while the evolution of the impedance for PEO-LDH and PEO-LDH-FA coatings is relatively stable during the EIS test (Fig. 12b and c). The addition of nanocontainers and inhibitor into the coatings result in well-defined capacitive loops on Nyquist diagrams. The high impedance at low frequency can be associated with the stability of the thin dense oxide layer present at the metal/coating interface and respectively an enhanced corrosion resistance. The value of low frequency impedance of the LDH loaded PEO coatings

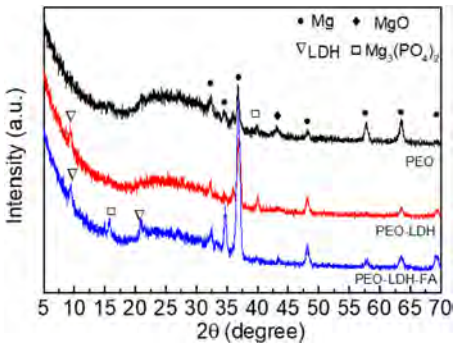

Fig. 9. Grazing angle XRD of the PEO coatings.

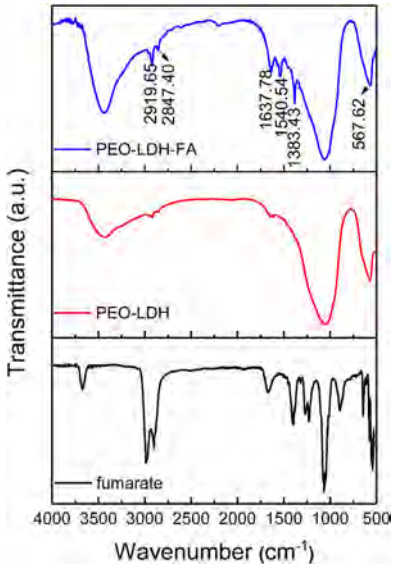

Fig. 10. ATR FT-IR spectra of fumarate, PEO-LDH and PEO-LDH-FA coating.

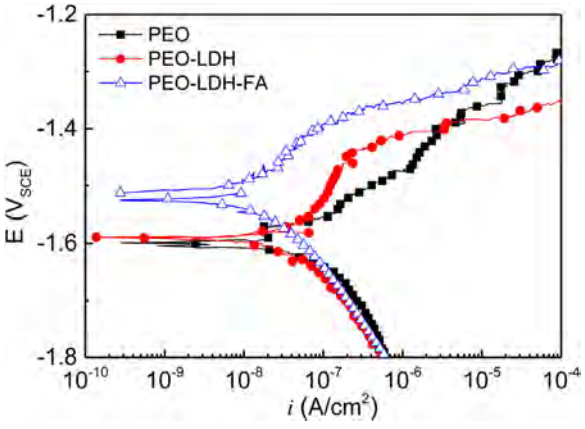

Fig. 11. Potentiodynamic polarization of the PEO coatings in 0.5 wt.% NaCl.

are more stable and kept at relatively high level throughout the entire immersion test, indicating that the LDH containing coatings have superior corrosion protection property.

To further understand the evolution of the corrosion resistance of the coatings, equivalent circuit (Fig. 13) was used to fit the impedance spectra and fitting data are shown in

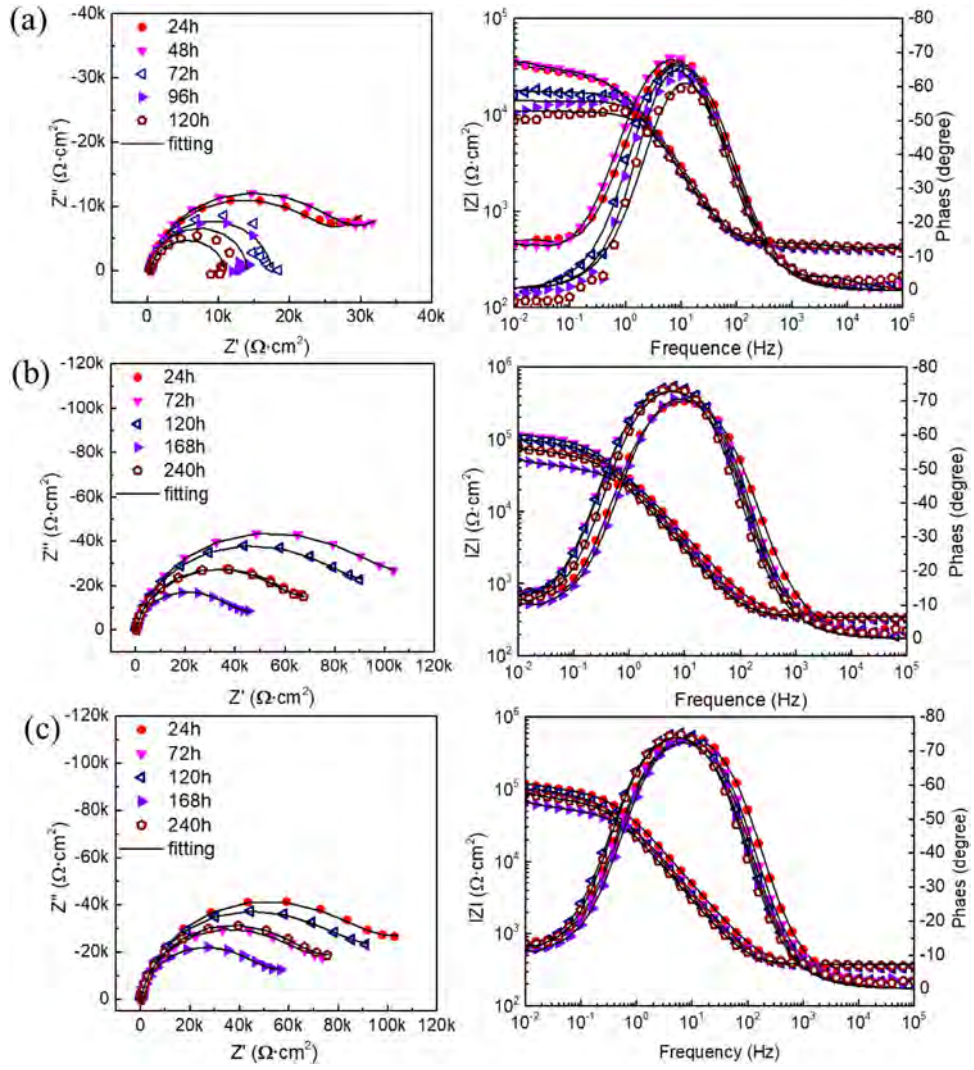

Fig. 12. Electrochemical impedance behavior of the PEO coatings in 0.5 wt.% NaCl (a) PEO (b) PEO-LDH (c) PEO-LDH-FA.

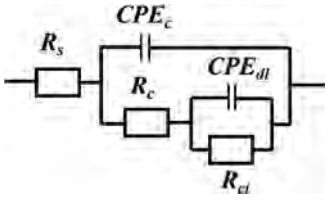

Fig. 13. Equivalent circuit used to fit the EIS data.

Table 4
Surface composition (at.%) of the corroded samples after performing EIS test.

Element	O	Mg	Al	P	Zn	Cl
PEO	66.04	25.02	2.21	6.45	n/a	0.28
PEO-LDH	57.23	20.90	3.40	15.92	2.23	0.32
PEO-LDH-FA	58.35	21.21	3.16	14.95	1.82	0.62

Table 3. R_s is solution resistance, R_c and CPE_c are resistance of the thin layer at the metal interface and its capacitance. R_{ct} and CPE_{dl} are related to the charge transfer resistance

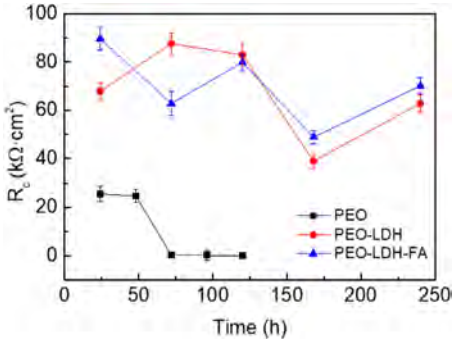

Fig. 14. Evolution of R_c of the different PEO coatings during EIS test.

and double layer capacitance at the electrolyte/metal interface. The evolution of R_c of the coatings during corrosion test is presented in Fig. 14. It can be seen that the resistance of the thin dense oxide layer is 25.6 kΩ cm^2 after immersion for 24 h, which is followed by continued decrease of coating performance. In contrast, it can be noticed that the R_c value of LDH containing coatings are much higher than

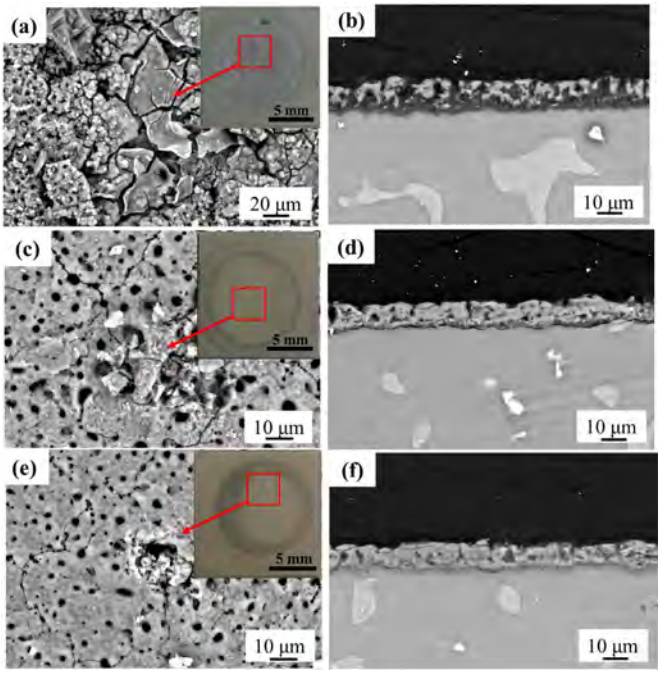

Fig. 15. Macroscopic, surface and cross-sectional morphology of the coatings after performing EIS test (a and b) PEO, (c and d) PEO-LDH and (e and f) PEO-LDH-FA.

that of blank PEO coating during the entire corrosion test. The starting value of R_c for PEO-LDH and PEO-LDH-FA is 67.8 and 89.7 kΩ cm^2, and remains to be at the same level afterwards.

This is probably associated with the inertly incorporated LDH nanocontainers, which have the ability to capture corrosive ions when corrosion occurs. The doped fumarate also plays a vital role in further enhancement of the corrosion resistance of the coating, since the inhibitors are exchanged and released from the nanocontainers to inhibit corrosion of Mg substrate.

3.7. Microstructure and morphology of the corroded coatings

Fig. 15 shows the macroscopic and microscopic morphology of the corroded samples after EIS test. As expected, corrosion products are accumulated on the surface of the blank PEO coating (Fig. 15a), while the LDH containing coatings appear to be intact and still protective (Fig. 15c and e). It can be seen that the blank coating is severely corroded and covered by large fraction of corrosion products. The coatings degrade slightly after 10 days immersion test in the presence of LDH nanocontainers (Fig. 15c and e). The original pores are still observable on the coating surface (Fig. 15e). The cross section of the layer confirms that the LDH containing coatings are still intact after corrosion test, while the blank PEO coating is almost completely corroded. The elemental composition of the corroded samples was showed in Table 4. It is apparent that the *P* content in the coating is greatly reduced, suggesting that the original layer is dissolved after corrosion test. Another interesting phenomenon is that

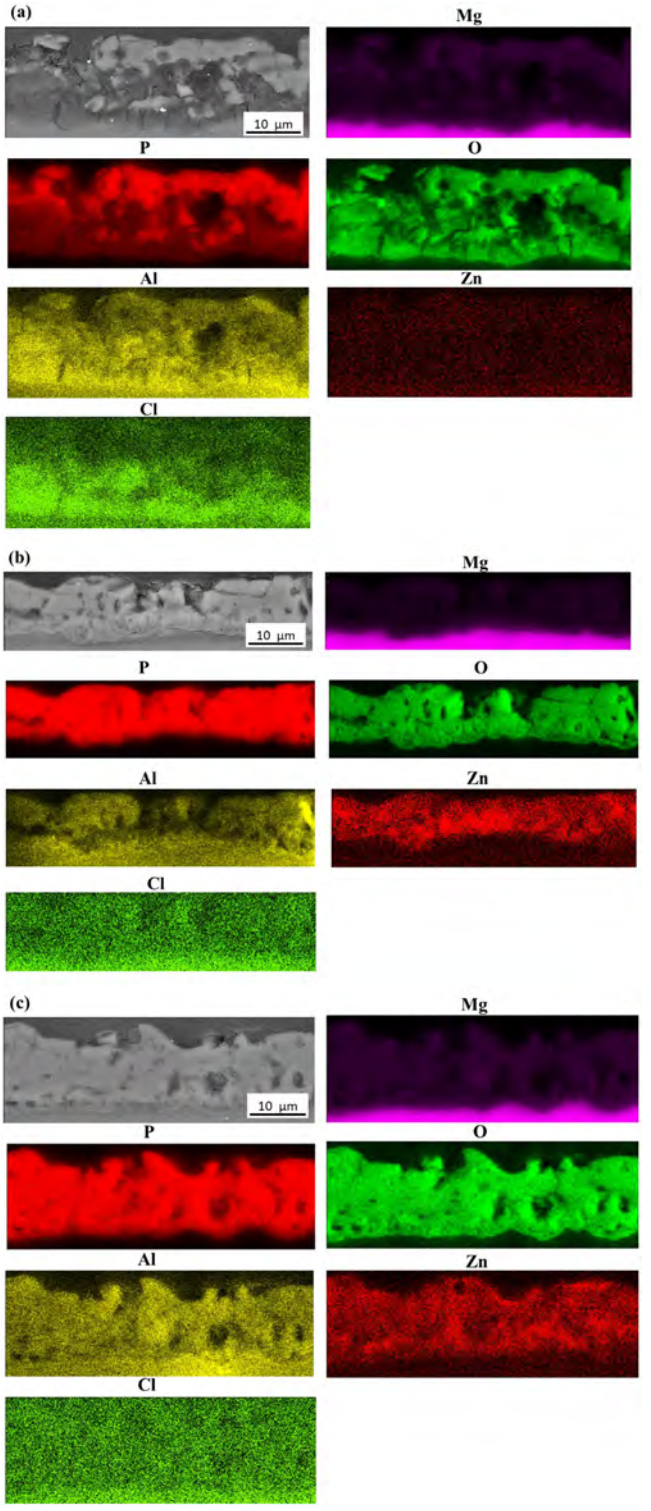

Fig. 16. EDS mapping of the corroded samples after performing EIS test (a) PEO, (b) PEO-LDH and (c) PEO-LDH-FA.

although the PEO-LDH and PEO-LDH-FA coatings are not severely degraded, the content of the Cl ions in the coating is higher compared to that of the blank PEO coating, indicating that the incorporated LDH nanocontainers are capable of capturing corrosive ions during corrosion test. Moreover,

the fumarate containing coating appears to be more compact and protective after EIS test compared to the other two types of coatings, which can be proved by the intact coating/metal interface. It can be inferred that the doped corrosion inhibitor is still active and able to inhibit the coating degradation. The elemental EDS maps of the cross section of the corroded samples were demonstrated in Fig. 16. It can be found that the blank PEO coating is severely corroded, as reflected by the porous and fractured layer. Strong Cl signal is detected in the corroded coating, which is hardly to be observable for nanocontainer containing coatings (Fig. 16b and c).

3.8. Formation and degradation process of the coatings

Based on the above analysis, it can be concluded that anionic corrosion inhibitor is loaded into the interlayer of LDH nanocontainers, which can be subsequently incorporated into the layer to greatly enhance the corrosion resistance of the PEO coating, since the corrosive ions can be exchanged and captured by nanocontainers to suppress corrosion. The presence of LDH nanocontainers and corrosion inhibitor accelerates the coating growth rate and results in formation of dense and protective PEO coating. Although corrosion inhibitor can be loaded into nanocontainer and be incorporated into the layer, the enhancement of corrosion performance of PEO coating is not that remarkable, which might be due to insufficient loading efficiency and the destructive effect of the high-energy discharges during coating formation process. Further investigation on controllable loading of corrosion inhibitors is of great importance to provide active and long-term corrosion protection for Mg surfaces.

4. Conclusions

In the present study, *in-situ* incorporation of LDH nanocontainers has been achieved for PEO coatings on AZ91 Mg alloy. A specific corrosion inhibitor (fumarate) is exchanged and intercalated into the nanocontainers, which have been subsequently incorporated into the layer during coating formation process. The coatings become thicker and denser after addition of LDH. The corrosion resistance of the LDH containing coatings remains to be stable and superior compared with the blank coating. The degradation process and corrosion resistance of PEO coating are found to be influenced by the loaded inhibitor and nanocontainers, leading to enhanced and stable corrosion performance in NaCl solution.

Declaration of Competing Interest

The authors declare that they have no known competing financial interests or personal relationships that could have appeared to influence the work reported in this paper.

Acknowledgments

The authors would like to acknowledge the financial support from National Natural Science Foundation of China (No. 52071067 and U1737102), Mobility Programme of the Sino-German Center (M-0056), the Fundamental Research Funds for the Central Universities (N2002009) and FUNCOAT project (H2020-MSCA-RISE-2018, Grant Agreement N 823942).

References

[1] M. Esmaily, J.E. Svensson, S. Fajardo, N. Birbilis, G.S. Frankel, S. Virtanen, R. Arrabal, S. Thomas, L.G. Johansson, Fundamentals and advances in magnesium alloy corrosion, Prog Mater Sci 89 (2017) 92–193.
[2] Y. Zhang, P. Gore, W. Rong, Y. Wu, Y. Yan, R. Zhang, L. Peng, J.-F. Nie, N. Birbilis, Quasi-in-situ STEM-EDS insight into the role of Ag in the corrosion behaviour of Mg-Gd-Zr alloys, Corros Sci 136 (2018) 106–118.
[3] M.P. Gomes, I. Costa, N. Pébère, J.L. Rossi, B. Tribollet, V. Vivier, On the corrosion mechanism of Mg investigated by electrochemical impedance spectroscopy, Electrochim Acta 306 (2019) 61–70.
[4] M. Jönsson, D. Thierry, N. LeBozec, The influence of microstructure on the corrosion behaviour of AZ91D studied by scanning Kelvin probe force microscopy and scanning Kelvin probe, Corros Sci 48 (5) (2006) 1193–1208.
[5] J. Song, J. She, D. Chen, F. Pan, Latest research advances on magnesium and magnesium alloys worldwide, J Magnes Alloy 8 (1) (2020) 1–41.
[6] Z. Shi, G. Song, A. Atrens, The corrosion performance of anodised magnesium alloys, Corros Sci 48 (11) (2006) 3531–3546.
[7] G. Williams, H.N. McMurray, R. Grace, Inhibition of magnesium localised corrosion in chloride containing electrolyte, Electrochim Acta 55 (27) (2010) 7824–7833.
[8] A. Pardo, M.C. Merino, A.E. Coy, R. Arrabal, F. Viejo, E. Matykina, Corrosion behaviour of magnesium/aluminium alloys in 3.5wt.% NaCl, Corros Sci 50 (3) (2008) 823–834.
[9] G.L. Song, 1 - Corrosion electrochemistry of magnesium (Mg) and its alloys, in: G.-l. Song (Ed.), Corrosion of Magnesium Alloys, Woodhead Publishing, 2011, pp. 3–65.
[10] P. Liu, J.-M. Wang, X.-T. Yu, X.-B. Chen, S.-Q. Li, D.-C. Chen, S.-K. Guan, R.-C. Zeng, L.-Y. Cui, Corrosion resistance of bioinspired DNA-induced Ca–P coating on biodegradable magnesium alloy, J Magnes Alloy 7 (1) (2019) 144–154.
[11] G. Duan, L. Yang, S. Liao, C. Zhang, X. Lu, Y. Yang, B. Zhang, Y. Wei, T. Zhang, B. Yu, X. Zhang, F. Wang, Designing for the chemical conversion coating with high corrosion resistance and low electrical contact resistance on AZ91D magnesium alloy, Corros Sci 135 (2018) 197–206.
[12] Z.-H. Xie, D. Li, Z. Skeete, A. Sharma, C.-J. Zhong, Nanocontainer-Enhanced Self-Healing for Corrosion-Resistant Ni Coating on Mg Alloy, ACS Appl Mater Interfaces 9 (41) (2017) 36247–36260.
[13] N.V. Murillo-Gutiérrez, F. Ansart, J.P. Bonino, M.J. Menu, M. Gressier, Protection against corrosion of magnesium alloys with both conversion layer and sol–gel coating, Surf Coat Technol 232 (2013) 606–615.
[14] A.L. Yerokhin, X. Nie, A. Leyland, A. Matthews, S.J. Dowey, Plasma electrolysis for surface engineering, Surf Coat Technol 122 (2) (1999) 73–93.
[15] J. Liang, P.B. Srinivasan, C. Blawert, W. Dietzel, Comparison of electrochemical corrosion behaviour of MgO and ZrO2 coatings on AM50 magnesium alloy formed by plasma electrolytic oxidation, Corros Sci 51 (10) (2009) 2483–2492.
[16] R.O. Hussein, X. Nie, D.O. Northwood, An investigation of ceramic coating growth mechanisms in plasma electrolytic oxidation (PEO) processing, Electrochimica Acta 112 (2013) 111–119.
[17] X. Lu, C. Blawert, D. Tolnai, T. Subroto, K.U. Kainer, T. Zhang, F. Wang, M.L. Zheludkevich, 3D reconstruction of plasma electrolytic oxidation coatings on Mg alloy via synchrotron radiation tomography, Corros Sci 139 (2018) 395–402.
[18] G. Rapheal, S. Kumar, N. Scharnagl, C. Blawert, Effect of current density on the microstructure and corrosion properties of plasma electrolytic oxidation (PEO) coatings on AM50 Mg alloy produced in an electrolyte containing clay additives, Surf Coat Technol 289 (2016) 150–164.

[19] J. Liang, P.B. Srinivasan, C. Blawert, M. Störmer, W. Dietzel, Electrochemical corrosion behaviour of plasma electrolytic oxidation coatings on AM50 magnesium alloy formed in silicate and phosphate based electrolytes, Electrochimica Acta 54 (14) (2009) 3842–3850.
[20] A. Jangde, S. Kumar, C. Blawert, Evolution of PEO coatings on AM50 magnesium alloy using phosphate-based electrolyte with and without glycerol and its electrochemical characterization, J Magnes Alloy 8 (3) (2020) 692–715.
[21] X. Lu, M. Mohedano, C. Blawert, E. Matykina, R. Arrabal, K.U. Kainer, M.L. Zheludkevich, Plasma electrolytic oxidation coatings with particle additions – A review, Surf Coat Technol 307 (2016) 1165–1182.
[22] R. Arrabal, E. Matykina, F. Viejo, P. Skeldon, G.E. Thompson, Corrosion resistance of WE43 and AZ91D magnesium alloys with phosphate PEO coatings, Corros Sci 50 (6) (2008) 1744–1752.
[23] Y. Chen, X. Lu, C. Blawert, M.L. Zheludkevich, T. Zhang, F. Wang, Formation of self-lubricating PEO coating via in-situ incorporation of PTFE particles, Surf Coat Technol 337 (2018) 379–388.
[24] J. Zhao, X. Xie, C. Zhang, Effect of the graphene oxide additive on the corrosion resistance of the plasma electrolytic oxidation coating of the AZ31 magnesium alloy, Corros Sci 114 (2017) 146–155.
[25] X. Lu, C. Blawert, K.U. Kainer, T. Zhang, F. Wang, M.L. Zheludkevich, Influence of particle additions on corrosion and wear resistance of plasma electrolytic oxidation coatings on Mg alloy, Surf Coat Technol 352 (2018) 1–14.
[26] A. Castellanos, A. Altube, J.M. Vega, E. García-Lecina, J.A. Díez, H.J. Grande, Effect of different post-treatments on the corrosion resistance and tribological properties of AZ91D magnesium alloy coated PEO, Surf Coat Technol 278 (2015) 99–107.
[27] L. Chen, Y. Sheng, H. Zhou, Z. Li, X. Wang, W. Li, Influence of a MAO + PLGA coating on biocorrosion and stress corrosion cracking behavior of a magnesium alloy in a physiological environment, Corros Sci 148 (2019) 134–143.
[28] X. Zheng, Q. Liu, H. Ma, S. Das, Y. Gu, L. Zhang, Probing local corrosion performance of sol-gel/MAO composite coating on Mg alloy, Surf Coat Technol 347 (2018) 286–296.
[29] S. Wang, X. Guo, Y. Xie, L. Liu, H. Yang, R. Zhu, J. Gong, L. Peng, W. Ding, Preparation of superhydrophobic silica film on Mg–Nd–Zn–Zr magnesium alloy with enhanced corrosion resistance by combining micro-arc oxidation and sol–gel method, Surf Coat Technol 213 (2012) 192–201.
[30] S.V. Lamaka, G. Knörnschild, D.V. Snihirova, M.G. Taryba, M.L. Zheludkevich, M.G.S. Ferreira, Complex anticorrosion coating for ZK30 magnesium alloy, Electrochimica Acta 55 (1) (2009) 131–141.
[31] Y. Chen, X. Lu, S.V. Lamaka, P. Ju, C. Blawert, T. Zhang, F. Wang, M.L. Zheludkevich, Active protection of Mg alloy by composite PEO coating loaded with corrosion inhibitors, Appl Surf Sci (2019) 144462.
[32] K. Qian, W. Li, X. Lu, X. Han, Y. Jin, T. Zhang, F. Wang, Effect of phosphate-based sealing treatment on the corrosion performance of a PEO coated AZ91D mg alloy, J Magnes Alloy 8 (4) (2020) 1328–1340.
[33] J. Yang, C. Blawert, S.V. Lamaka, D. Snihirova, X. Lu, S. Di, M.L. Zheludkevich, Corrosion protection properties of inhibitor containing hybrid PEO-epoxy coating on magnesium, Corros Sci 140 (2018) 99–110.
[34] D. Ivanou, K. Yasakau, S. Kallip, A.D. Lisenkov, M. Starykevich, S.V. Lamaka, M. Ferreira, M.L. Zheludkevich, Active corrosion protection coating for ZE41 magnesium alloy created by combining PEO and sol-gel techniques, RSC Adv 6 (2016) 12553–12560.
[35] M. Sun, A. Yerokhin, M.Y. Bychkova, D.V. Shtansky, E.A. Levashov, A. Matthews, Self-healing plasma electrolytic oxidation coatings doped with benzotriazole loaded halloysite nanotubes on AM50 magnesium alloy, Corros Sci 111 (2016) 753–769.
[36] M.L. Zheludkevich, J. Tedim, M.G.S. Ferreira, Smart" coatings for active corrosion protection based on multi-functional micro and nanocontainers, Electrochimica Acta 82 (2012) 314–323.
[37] M.F. Montemor, Functional and smart coatings for corrosion protection: A review of recent advances, Surf Coat Technol 258 (2014) 17–37.
[38] D. Evans, R. Slade, Structural Aspects of Layered Double Hydroxides 119 (2005) 1–87.
[39] X. Wang, C. Jing, Y. Chen, X. Wang, G. Zhao, X. Zhang, L. Wu, X. Liu, B. Dong, Y. Zhang, Active corrosion protection of super-hydrophobic corrosion inhibitor intercalated Mg–Al layered double hydroxide coating on AZ31 magnesium alloy, J Magnes Alloy 8 (1) (2020) 291–300.
[40] M.L. Zheludkevich, S.K. Poznyak, L.M. Rodrigues, D. Raps, T. Hack, L.F. Dick, T. Nunes, M.G.S. Ferreira, Active protection coatings with layered double hydroxide nanocontainers of corrosion inhibitor, Corros Sci 52 (2) (2010) 602–611.
[41] M. Abdolah Zadeh, J. Tedim, M. Zheludkevich, S. van der Zwaag, S.J. Garcia, Synergetic active corrosion protection of AA2024-T3 by 2D- anionic and 3D-cationic nanocontainers loaded with Ce and mercaptobenzothiazole, Corros Sci 135 (2018) 35–45.
[42] F. Peng, H. Li, D. Wang, P. Tian, Y. Tian, G. Yuan, D. Xu, X. Liu, Enhanced Corrosion Resistance and Biocompatibility of Magnesium Alloy by Mg–Al-Layered Double Hydroxide, ACS Appl Mater Interfaces 8 (51) (2016) 35033–35044.
[43] M. Serdechnova, M. Mohedano, B. Kuznetsov, C.L. Mendis, M. Starykevich, S. Karpushenkov, J. Tedim, M.G.S. Ferreira, C. Blawert, M.L. Zheludkevich, PEO Coatings with Active Protection Based on In-Situ Formed LDH-Nanocontainers, J Electrochem Soc 164 (2) (2017) C36–C45.
[44] M. Mohedano, M. Serdechnova, M. Starykevich, S. Karpushenkov, A.C. Bouali, M.G.S. Ferreira, M.L. Zheludkevich, Active protective PEO coatings on AA2024: Role of voltage on in-situ LDH growth, Mater Des 120 (2017) 36–46.
[45] L. Wu, G. Zhang, A. Tang, X.-B. Chen, Y. Ma, Y. Long, P. Peng, X. Ding, H. Pan, F.-S. Pan, Growth behavior of MgAl-layered double hydroxide films by conversion of anodic films on magnesium alloy AZ31 and their corrosion protection, Appl Surf Sci 456 (2018) 419–429.
[46] G. Zhang, L. Wu, A. Tang, Y. Ma, G.-L. Song, D. Zheng, B. Jiang, A. Atrens, F. Pan, Active corrosion protection by a smart coating based on a MgAl-layered double hydroxide on a cerium-modified plasma electrolytic oxidation coating on Mg alloy AZ31, Corros Sci 139 (2018) 370–382.
[47] E. Petrova, M. Serdechnova, T. Shulha, S.V. Lamaka, D.C.F. Wieland, P. Karlova, C. Blawert, M. Starykevich, M.L. Zheludkevich, Use of synergistic mixture of chelating agents for in situ LDH growth on the surface of PEO-treated AZ91, Sci Rep 10 (1) (2020) 8645.
[48] A.C. Bouali, M.H. Iuzviuk, M. Serdechnova, K.A. Yasakau, D.C.F. Wieland, G. Dovzhenko, H. Maltanava, I.A. Zobkalo, M.G.S. Ferreira, M.L. Zheludkevich, Zn-Al LDH growth on AA2024 and zinc and their intercalation with chloride: Comparison of crystal structure and kinetics, Appl Surf Sci 501 (2020) 144027.
[49] J. Yang, C. Blawert, S.V. Lamaka, K.A. Yasakau, L. Wang, D. Laipple, M. Schieda, S. Di, M.L. Zheludkevich, Corrosion inhibition of pure Mg containing a high level of iron impurity in pH neutral NaCl solution, Corros Sci 142 (2018) 222–237.
[50] L.I. Fockaert, T. Würger, R. Unbehau, B. Boelen, R.H. Meißner, S.V. Lamaka, M.L. Zheludkevich, H. Terryn, J.M.C. Mol, ATR-FTIR in Kretschmann configuration integrated with electrochemical cell as in situ interfacial sensitive tool to study corrosion inhibitors for magnesium substrates, Electrochimica Acta 345 (2020) 136166.
[51] T. Zhang, Y. Li, F. Wang, Roles of β phase in the corrosion process of AZ91D magnesium alloy, Corros Sci 48 (5) (2006) 1249–1264.
[52] M. Serdechnova, A.N. Salak, F.S. Barbosa, D.E.L. Vieira, J. Tedim, M.L. Zheludkevich, M.G.S. Ferreira, Interlayer intercalation and arrangement of 2-mercaptobenzothiazolate and 1,2,3-benzotriazolate anions in layered double hydroxides: In situ X-ray diffraction study, J Solid State Chem 233 (2016) 158–165.
[53] M.V. Bukhtiyarova, A review on effect of synthesis conditions on the formation of layered double hydroxides, J Solid State Chem 269 (2019) 494–506.
[54] S. Koosehgol, M. Ebrahimian-Hosseinabadi, M. Alizadeh, A. Zamanian, Preparation and characterization of in situ chitosan/polyethylene glycol fumarate/thymol hydrogel as an effective wound dressing, Mater Sci Eng C 79 (2017) 66–75.
[55] Z. Karami, M. Jouyandeh, J.A. Ali, M.R. Ganjali, M. Aghazadeh, S.M.R. Paran, G. Naderi, D. Puglia, M.R. Saeb, Epoxy/layered dou-

ble hydroxide (LDH) nanocomposites: Synthesis, characterization, and Excellent cure feature of nitrate anion intercalated Zn-Al LDH, Prog Org Coat 136 (2019) 105218.

[56] E. McCafferty, Validation of corrosion rates measured by the Tafel extrapolation method, Corros Sci 47 (12) (2005) 3202–3215.

[57] Y. Chen, Y. Yang, T. Zhang, W. Zhang, F. Wang, X. Lu, C. Blawert, M.L. Zheludkevich, Interaction effect between different constituents in silicate-containing electrolyte on PEO coatings on Mg alloy, Surf Coat Technol 307 (2016) 825–836.